Joint Special Interest Group meeting between euspen and ASPE
Advancing Precision in Additive Manufacturing
KU Leuven, Belgium, September 2023
www.euspen.eu

In-situ fringe projection profilometry and spatter monitoring data fusion to predict mechanical properties in laser powder bed fusion additive manufacturing

Haolin Zhang[1], Alexander N Caputo[2], Heyang Zhang[1], Md Mahmudul Hasan[1], Chaitanya Vallabh[1], Richard W Neu[2], Xiayun Zhao[1]

[1]*Department of Mechanical Engineering and Materials Science, University of Pittsburgh Pittsburgh, Pennsylvania 15261, USA*
[2]*George W. Woodruff School of Mechanical Engineering, Georgia Institute of Technology, Atlanta, Georgia 30332, USA*

xiayun.zhao@pitt.edu

Abstract
Laser powder bed fusion (LPBF) additive manufacturing has the potential of efficiently producing components with high resolution and complex geometry. However, during LPBF the as-manufactured layers usually possess rough surfaces due to spattering and other mechanisms that lead to porosity formation and unsatisfactory mechanical properties, necessitating extensive post-processing prior to being deployed for practical applications. Fringe projection profilometry (FPP) is a cost-effective, non-invasive technology that has been developed for in-situ LPBF surface measurement. This work is aimed to develop a joint monitoring system that combines in-situ FPP and spatter monitoring systems to extract in-process layer surface features alongside melt pool spattering signatures, which together can serve as relatively comprehensive implications of potential defects that could be caused by spatters, balling, or shrinkage. Then, multiple regression models are developed to correlate the FPP-measured thickness profiles and the inferred layer-wise surface defects with the ex-situ characterized part properties including hardness, and fatigue life. The proposed multi-monitoring framework can help optimize or control LPBF processes for achieving improved mechanical properties.

Keywords: Laser Powder Bed Fusion, Process Monitoring, Optical Profilometry, Data Fusion

1. Introduction

Laser powder bed fusion (LPBF) additive manufacturing (AM) process utilizes the laser as the energy input to sinter or melt metal powders for fabricating complicated designs with high resolution. This technology has been widely used in industries such as aerospace and automobile due to its flexibility and suitability for rapid prototyping. However, LPBF faces challenges in attaining desired mechanical properties such as long fatigue life, good surface quality, and high part density ratio due to the complex physics interplays between powder, laser, and fused part.

Spatter, a characteristic phenomenon of LPBF process, is the ejected materials from the melt pool (MP) induced primarily by the recoil pressure and Marangoni effect [1]. The redeposition of spatters is one of the main sources causing rough layer-wise surfaces and the formation of lack of fusion porosity [2, 3]. Furthermore, the generation of the spatters also indicates the processing regimes such as transition, keyholing, and lack of fusion. Spatters are divided into solid spatter, metallic jet, entrainment melting spatter, and defect induced spatter based on the previous studies [4]. Because of the detrimental effects of spatters, there is a significant need to develop monitoring or simulation methods to characterize and quantify the impacts of spatters on part properties. However, state-of-the-art simulation is expensive in computation time, making it not suitable for part-scale modeling. As a cost-effective solution, off-axis camera monitoring is broadly used to study the generation of the spatters from the melt pool, but faces challenges to capture the whole dynamics from ejection to landing [5, 6].

Surface roughness is an important metric used to evaluate the quality of printed samples, and can be determined by surface topography, which can provide information about surface defects including recoater crash, surface porosity, and redeposited spatters [7]. It is essential to monitor the layer-wise surface topography during the printing process to qualify the final printed part. Fringe projection profilometry (FPP) is the structure light projection methodology which has recently been adopted to monitor in-situ surface topography for LPBF [8, 9]. The FPP system is a non-contact metrology which is capable of acquiring high-resolution height map of the target geometry in relatively short time, making it suitable for monitoring LPBF manufacturing processes. The basic system is composed of a projector and a camera. The projector projects sinusoidal patterns to the target, and the camera captures the pattern which is distorted by the target geometry. Most of the research performed in using FPP to monitor LPBF process focuses on improving measurement accuracy. For example, researchers have investigated the impact of the camera and projector angle on the final measurement performance [10]. However, there is a lack of study on investigating or correlating the measured layer-wise surface topography to mechanical properties of the printed part.

In sum, this work aims to utilize the spatters and surface topography monitored by the lab-designed multi-modal monitoring systems to predict printed part's mechanical properties including fatigue life, hardness, and critical crack location. The developed model will first extract surface

topography and spatter features, and then fuse these quantified features for analyzing their correlations to mechanical properties. The developed model will assist the real-time control of the process by revealing the roles of the spatters and the surface topography on defects and properties.

2. Methodology

In this work, an in-house FPP system and method is implemented for surface topography measurement. Meanwhile, an off-axis high-speed camera is used for capturing the spatters. The systems setup on the commercial EOS M290 LPBF machine is shown in Figure 1.

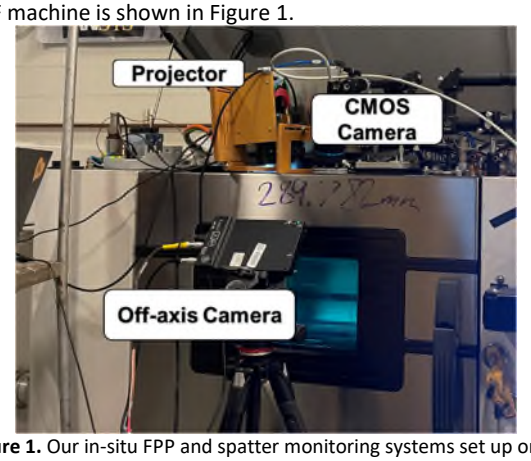

Figure 1. Our in-situ FPP and spatter monitoring systems set up on an EOS M290 laser powder bed fusion printer

2.1. Fringe Projection Profilometry System

The FPP system has one DLP projector (LightCrafter 4710 EVM G2, Texas Instruments, Dallas, TX) and one CMOS monochrome camera (BFS-U3-120S4M-CS USB 3.1 Blackfly). Three sinusoidal patterns are projected to the build area during the printing with phase shift of $0\,\pi, \frac{2}{3}\pi$, and $\frac{4}{3}\pi$. The three-step phase shifting algorithm is used to compute the wrapped phase value.

$$I(x,y) = B(x,y) + M(x,y)\cos\left(\phi(x,y) + \delta\right) \tag{1}$$

$$I_{Calibrated} = \frac{I_{Camera}}{C_{xy}}, C_{xy} = \frac{I^{Camera}}{I^{Projected}} \tag{2}$$

$$\phi(x,y) = \arctan\left(\frac{-\sum_{i-1}^{N} I_i^{Calibrated}(x,y)\sin\left(\delta_i\right)}{\sum_{i-1}^{N} I_i^{Calibrated}(x,y)\cos\left(\delta_i\right)}\right) \tag{3}$$

Shown in Equation (1), the camera captured intensity at the given pixel location x and y ($I(x,y)$) is the function of ambient background intensity B, projector bias M, and wrapped phase value ϕ. δ is the phase shift of the projected pattern. For FPP system, one major phase error source is from the camera and projector nonlinearity. To account for the nonlinearity between the projected intensity and camera captured intensity, the correction factor C_{xy} is implemented as presented in Equation (2). The value of C_{xy} is determined empirically by projecting 20 even-spaced different grayscale intensities from 0 to 255. The two-dimensional Fast Fourier Transform (2D FFT) filter is used to reduce the phase jump error after phase unwrapping stage. In this work, the linear model is used to calibrate the unwrapped phase to height relation.

2.2. Off-axis Camera Spatter Monitoring and Machine Learning aided Data Processing

The high-seed CMOS camera (Fastec IL5Q) is installed outside of the building chamber at an angle (Figure 1) to capture the melt pool and spatters generation with the resolution of 640×512 pixels. The spatial coordinates of the melt pool is registered using the framework developed in our previous work [3]. After the spatial coordinate registration, the perspective corrected images are cropped to focus on the MP and ejected spatters. The semantic segmentation neural network is then used to label the pixels into three categories (background, melt pool, and spatters). The neural network is the DeepLabv3 convolutional neural network (CNN) with Atrous convolution [11]. The model is trained with manually labelled images from MPs of different processing regimes including transition, keyhole, and lack of fusion. Unlike the standard convolution operation, Atrous convolution is used which the convolution filter is dilated with certain strides. This design allows the convolution filter to have a broad field of view and consider features with flexible resolution. For the standard 1 channel grayscale image data, the output feature map is computed as:

$$y_i = \sum_k x_{i+r\cdot k} W_k \tag{4}$$

r is the dilated stride, and k is the kernel size. When the dilated stride is 1, the convolution filter is identical to the standard depth-wise convolution kernel filter.

In this work, spatter count is extracted from the segmented MP images using Density-based spatial clustering of applications with noise (DBSCAN). For more details on the spatter registration, please refer to our previous work [12].

2.3. Ex-situ Mechanical Testing

2.3.1 High Cycle Fatigue Testing

All testing in this work was conducted in force control on an MTS model 370 servohydraulic test system (Eden Prairie, MN, USA). Specimens were gripped using hydraulic wedge grips with serrated steel inserts using 1/16" thick garolite shims to prevent fatigue specimens from fracture in the grip sections. Guides were used to insure alignment of fatigue specimens between the wedge grips. The guides were installed using a flat calibration specimen and a level to insure vertical alignment of fatigue specimens. The high cycle fatigue (HCF) test conditions comprised of a stress ratio (R) of 0.1, a maximum stress ($\sigma_{\max}$) of 500 MPa, and a loading frequency of 20 Hz with a sinusoidal wave form in lab air.

2.3.2 Hardness Testing

Vickers hardness testing was conducted in accordance with ASTM E384 on the grip regions of all specimens (polished up to 400 grit) using a LECO LM248AT Microhardness Tester with 500 gf weight applied. Each specimen was indented 20 separate times and all indentations were measured using the integrated optical microscope of the LECO LM248AT system.

3. Experiment Design

To investigate the effects of spattering and layer-wise surface topography on the mechanical properties of the printed part, five fatigue test samples (fatigue bars) are printed using the commercial EOS M290 laser powder bed fusion machine. The printing material is a commercial Ni-Cr super alloy (Inconel 718) metal powder. All the test samples are designed based on the ASTM E466 standards, and the default nominal setting are used including laser power of 285 W, laser scan speed of 960 mm/s, layer thickness of 40 μm, and hatching distance of 110 μm with 67 degrees of scan angle rotation. The strip hatching pattern is enabled with a strip width of 10 mm. In this work, the off-axis camera data is acquired at 1000 frame rate per second (fps), and the field of view is 200 mm × 180 mm on the built plane.

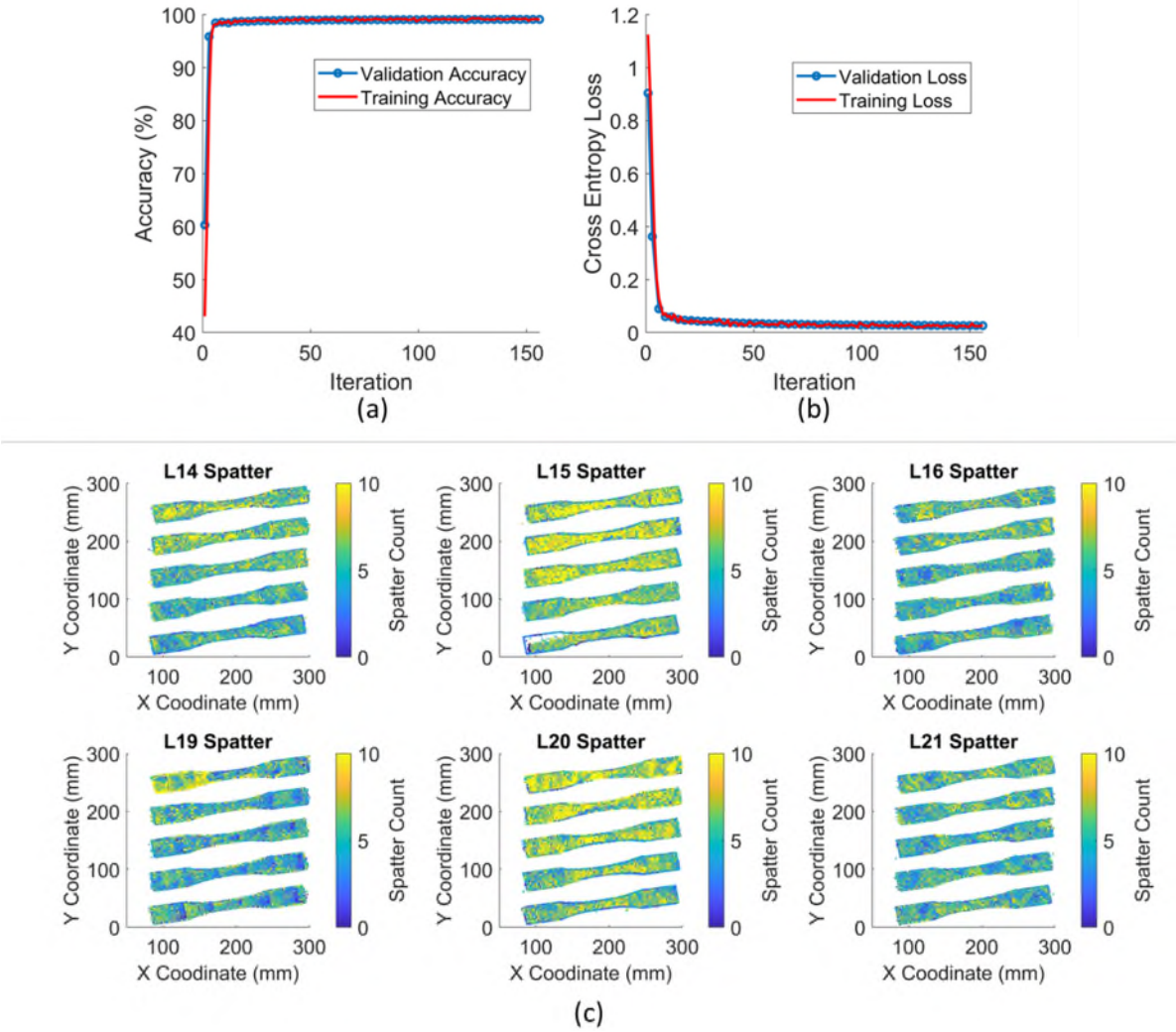

Figure 2. Machine learning aided spatter registration training and sample results. (a) Training and validation accuracy history (b) Training and validation loss histories; (c) Sample spatter count signature map for six layers monitored

4. Results and Discussion

In this section, data registration results for spatters, and regression analysis between fused signatures and ex-situ characterized mechanical properties including fatigue life and hardness are performed.

4.1. Machine Learning aided Spatter Registration

With the methods in Section 2.2, the machine learning model is trained on 1000 manually labelled images with the data split strategy of 70% for training, 10% for validation, and 20% for testing. The training and validation histories are shown in Figure 2, and the highest validation accuracy is 99.14% at iteration 144. The model with highest validation accuracy is saved and tested on the unseen test dataset, attaining the test accuracy of 99.18%. Sample results for the registered MP spatter count of six monitored layers are shown in Figure 2 (c). It is observed that spatter counts vary among different layers as the results of different hatching scan angles. Furthermore, the small number of spatters observed for the contour of fatigue bar suggests the relationship between spatters and nominal processing parameters (laser power and scan speed).

4.2 Regression Analysis between in-situ signatures and ex-situ Mechanical Properties

The areal surface roughness is computed as the signature from topography data acquired using FPP system.

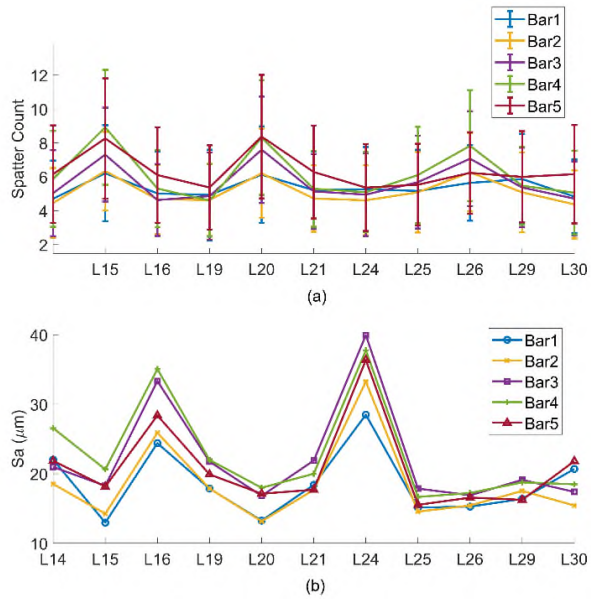

Figure 3. In-situ monitored signatures for the five fatigue test samples. x axis is the layer number. (a) Average spatter count; (b) Areal surface roughness (Sa)

Shown in Figure 3, both the average spatter count and areal surface roughness varies among different layers. Despite all the fatigue specimens are manufactured under same nominal processing parameters, in-situ data reveals that Sample 3 and Sample 4 result in larger Sa comparing to sample 1, 2, and 5. While Samples 3, 4, and 5 all present larger number of spatters monitored from Figure 3(a), it should be noted that the spatters captured by the off-axis camera is the spatter initiation but not the re-deposition. For this reason, the top to bottom gas flow is assumed to cause some spatters that are ejected from Sample 5 to land on Samples 3 and 4. The average layer-wise surface roughness, calculated as the arithmetic mean of all the layers' surface roughness (Sa), from Table 1 also suggests the potential defects formed due to poor surface quality from Samples 3 and 4.

Table 1. In-situ monitored signatures and ex-situ characterized Vicker;s Hardness and High Cycle Fatigue Life

Sample	Average Spatter Count	Average Surface Roughness (µm)	Vicker's Hardness (HV)	Fatigue Life (Cycles)
1	5.36	18.62	491.3	7.12E+6
2	5.13	18.50	500.4	9.30E+6
3	5.67	22.20	482.8	4.51E+6
4	6.17	22.83	487.2	4.00E+6
5	6.35	20.87	490.2	7.80E+6

Ex-situ characterized results show that Sample 3 and Sample 4 exhibit shorter fatigue life and lower hardness comparing to other samples. This observation is consistent with the observations from in-situ layer-wise surface roughness which sample 3 and 4 expose rougher surfaces. Regression analysis is then performed to correlate the in-situ signatures and ex-situ characterized properties. In this work, support vector machine (SVM), linear regression, and Gaussian process regression are used.

Table 2. Performances of Regression models with different metrics

Model	Objective	Root Mean Squared Error (RMSE)	Mean Absolute Error (MAE)	Mean Squared Error (MSE)
Support Vector Machine (SVM)	Hardness/Fatigue Life	2.84/2.8E+5	1.71/2.8E+5	8.07/7.8E+10
Linear Regression	Hardness/Fatigue Life	2.19/8.3E+5	1.87/7.0E+5	4.81/6.9E+11
Gaussian Process Regression	Hardness/Fatigue Life	2.50/2.8E+5	1.86/2.6E+5	6.24/8.2E+10

All the regression models reach high accuracy in correlating the bar-wise in-situ signatures and the ex-situ characterized fatigue life and Vicker's Hardness. This proves the importance of characterizing both spatters and surface roughness during the printing process, and their effects on the as-printed part properties. The experimental design also suggests that the dynamic LPBF manufacturing process is fluctuating, and samples with same nominal machine setting can exhibit significant different properties as reflected by the high-cycle fatigue and hardness tests.

5. Conclusion and Future work

This work developed a comprehensive monitoring system for laser powder fusion process to characterize in-process layer-wise surface topography and spatter ejection metrics. Further regression analysis reveals the relationship between these in-situ signatures to the fatigue life and hardness of printed sample. It is shown that ex-situ mechanical properties can be accurately inferred from the in-situ spatter count and layer-wise surface roughness. Future works include establishing a more generalized model by adding more experimental data for the regression analysis. Furthermore, current analysis is performed on bar-wise signatures, more studies on how to effectively use the layer-wise signatures to predict the ex-situ properties should be performed.

References

[1] H. Chen and W. Yan, "Spattering and denudation in laser powder bed fusion process: Multiphase flow modelling," *Acta Materialia,* vol. 196, pp. 154-167, 2020, doi: 10.1016/j.actamat.2020.06.033.

[2] R. Esmaeilizadeh, U. Ali, A. Keshavarzkermani, Y. Mahmoodkhani, E. Marzbanrad, and E. Toyserkani, "On the effect of spatter particles distribution on the quality of Hastelloy X parts made by laser powder-bed fusion additive manufacturing," *Journal of Manufacturing Processes,* vol. 37, pp. 11-20, 2019/01/01/ 2019, doi: https://doi.org/10.1016/j.jmapro.2018.11.012.

[3] H. Zhang, C. K. P. Vallabh, and X. Zhao, "Registration and fusion of large-scale melt pool temperature and morphology monitoring data demonstrated for surface topography prediction in LPBF," *Additive Manufacturing,* vol. 58, p. 103075, 2022/10/01/ 2022, doi: https://doi.org/10.1016/j.addma.2022.103075.

[4] D. Wang *et al.*, "Mechanisms and characteristics of spatter generation in SLM processing and its effect on the properties," *Materials & Design,* vol. 117, pp. 121-130, 2017.

[5] Y. Zhang, J. Y. H. Fuh, D. Ye, and G. S. Hong, "In-situ monitoring of laser-based PBF via off-axis vision and image processing approaches," *Additive Manufacturing,* vol. 25, pp. 263-274, 2019, doi: 10.1016/j.addma.2018.10.020.

[6] S. K. Everton, M. Hirsch, P. Stravroulakis, R. K. Leach, and A. T. Clare, "Review of in-situ process monitoring and in-situ metrology for metal additive manufacturing," *Materials & Design,* vol. 95, pp. 431-445, 2016, doi: 10.1016/j.matdes.2016.01.099.

[7] A. Triantaphyllou *et al.*, "Surface texture measurement for additive manufacturing," *Surface Topography: Metrology and Properties,* vol. 3, no. 2, 2015, doi: 10.1088/2051-672x/3/2/024002.

[8] B. Zhang, J. Ziegert, F. Farahi, and A. Davies, "In situ surface topography of laser powder bed fusion using fringe projection," *Additive Manufacturing,* vol. 12, pp. 100-107, 2016, doi: 10.1016/j.addma.2016.08.001.

[9] H. Zhang, C. K. P. Vallabh, Y. Xiong, and X. Zhao, "A systematic study and framework of fringe projection profilometry with improved measurement performance for in-situ LPBF process monitoring," *Measurement,* vol. 191, 2022, doi: 10.1016/j.measurement.2022.110796.

[10] N. M. O'Dowd, A. J. Wachtor, and M. D. Todd, "Effects of digital fringe projection operational parameters on detecting powder bed defects in additive manufacturing," *Additive Manufacturing,* vol. 48, 2021, doi: 10.1016/j.addma.2021.102454.

[11] L.-C. Chen, G. Papandreou, F. Schroff, and H. Adam, "Rethinking atrous convolution for semantic image segmentation," *arXiv preprint arXiv:1706.05587,* 2017.

[12] H. Zhang, C. K. P. Vallabh, and X. Zhao, "Influence of Spattering on In-process Layer Surface Roughness during Laser Powder Bed Fusion," *arXiv preprint arXiv:2303.00272,* 2023.